research papers

HRTEM study of orthorhombic zirconia in MgO-PSZ

Zongwen Liu,[a]* Yoshio Bando,[a] John Drennan[b] and Alan E. C. Spargo[c]

[a]Advanced Materials Laboratory, National Institute for Materials Science, Namiki 1-1, Tsukuba, Ibaraki 305-0044, Japan, [b]Centre for Microscopy and Microanalysis, The University of Queensland, Brisbane 4072, Australia, and [c]School of Physics, The University of Melbourne, Victoria 3010, Australia. Correspondence e-mail: liu.zongwen@nims.go.jp

High-resolution transmission electron microscopy (HRTEM) was used to study the phase of orthorhombic ZrO_2 formed in magnesia partially stabilized zirconia (MgO-PSZ) during HRTEM specimen preparation. Based on the three reported crystal structures of orthorhombic ZrO_2, with the space groups $Pbcm$, $Pbc2_1$ and $Pbca$, here it is shown that orthorhombic ZrO_2 formed in MgO-PSZ has the $Pbcm$ structure.

1. Introduction

MgO-PSZ is now one of the widely used industrial transformation-toughened ceramics. It is generally produced by the addition of the high-temperature soluble oxide stabilizer MgO to zirconia. The mixture is sintered at a temperature which is high enough to retain the cubic (c) single phase and then cooled at a controlled rate so that the precipitated 'pure zirconia' is in the metastable tetragonal (t) form at room temperature. They are then aged under suitable conditions to allow the tetragonal precipitates to grow to such a size that they will transform, at room temperature, to the monoclinic (m) form in the presence of an applied tensile stress field. The toughest MgO-PSZ is known to be obtained by subjecting the sintered and control-cooled material to a final sub-eutectoid aging treatment at 1373 K (Garvie *et al.*, 1981). It has been found that significant quantities of δ phase (Liu & Spargo, 2001*a*,*b*), with a composition of $Mg_2Zr_5O_{12}$, and small quantities of an orthorhombic (o) phase were formed during the sub-eutectoid heating (Hannink *et al.*, 1994). The δ phase is thought to be responsible for the increase in fraction toughness of MgO-PSZ ceramics by enhancing the metastability of the tetragonal precipitates (Hannink, 1983; Hannink *et al.*, 1994), whereas the presence of a large quantity of o phase will cause reduction in fracture toughness since o-ZrO_2 is not readily transformable by stress (Marshall *et al.*, 1989).

For a 9.8 mol% MgO-PSZ sample, a typical 'peak-aged' (2 h sub-eutectoid heating) bulk sample contains about 2.4% o phase (Hannink *et al.*, 1994). Larger quantities of o-ZrO_2 could be formed in MgO-PSZ by cooling (Marshall *et al.*, 1989), grinding (Hill & Reichert, 1990) and polishing (Suyama *et al.*, 1985; Liu, 1999). The o-ZrO_2 occurring from any of these treatments is believed to be transformed from tetragonal precipitates.

Three different structures for o-ZrO_2 have been reported. The first crystal structure determination was attempted by Kudoh *et al.* (1987) using a diamond anvil pressure cell and *in situ* single-crystal X-ray diffraction. The results showed that

the space group of o-ZrO_2 is $Pbcm$. Neutron diffraction studies (Kisi *et al.*, 1989; Howard *et al.*, 1991) of the o phase in cooled MgO-PSZ have shown that the low-temperature structure has space group $Pbc2_1$. Neutron diffraction work (Ohtaka *et al.*, 1990) on powders quenched from 873 K and 6 GPa showed that this high-temperature and high-pressure o phase has a structure with twice the a unit-cell parameter of the others, with space group $Pbca$. The parameters of the three structures are listed in Table 1.

A peak-aged (2 h sub-eutectoid heating) bulk sample contains about 2.4% o phase, 54.2% t phase, 22.1% c phase, 5.0% m phase and 16.3% δ phase (Hannink *et al.*, 1994). But TEM observation shows that the o phase is the most abundant phase (Fig. 1). Liu (1999) confirmed that most of the t phase was transformed to o phase during polishing and dimpling. The conclusion was drawn based on TEM observations of specimens prepared by different procedures. One specimen was prepared from an unpolished disc, which was directly thinned by an ion beam on both sides. As expected, HRTEM observation showed that the most abundant phase was the t phase. The other specimen was prepared from a disc which was polished on both sides. The polished disc was dimpled on one side and was then ion-beam thinned on the same side, while the other side of the disc was left untouched. HRTEM

Table 1
Crystal structure models for orthorhombic ZrO_2.

		Kudoh *et al.* (1987) $Pbcm$	Kisi *et al.* (1989) $Pbc2_1$	Ohtaka *et al.* (1990) $Pbca$
Zr	x	0.2683 (8)	0.267 (1)	0.2686 (2)
	y	0.0334 (2)	0.030 (1)	0.0332 (3)
	z	1/4	0.250 (1)	0.2558 (6)
O1	x	0.0822 (79)	0.068 (1)	0.0822 (6)
	y	0.3750 (21)	0.361 (1)	0.3713 (6)
	z	0.1292 (22)	0.106 (1)	0.1310 (5)
O2	x	0.4564 (54)	0.537 (1)	0.5442 (4)
	y	1/4	0.229 (1)	0.2447 (8)
	z	0	0	0.0052 (6)

observation indicated that most of the *t*-phase precipitates were transformed to *o* phase during specimen preparation. Thus, it is evident that the *t* to *o* transformation was induced by polishing and dimpling.

By taking a structure image combined with image simulation and digital Fourier transformation, here we show that *o*-ZrO₂ formed in MgO-PSZ as a result of polishing and dimpling can only have the *Pbcm* structure.

2. Materials and methods

MgO-PSZ containing 9.8 mol% MgO was prepared from mixed powders of the component oxides. The powder was sintered and solution-treated at 1973 K, cooled at 275 K h⁻¹ to 1273 K, and then at 70 K h⁻¹ to room temperature. The sample was reheated to 1373 K in air, aged for 2 h, and then furnace-cooled.

Thin foils of the sample were prepared for electron microscopy. A plate of about 1 mm thickness was cut from the sample using a diamond saw. The plate was polished on both sides. Small discs of 3 mm in diameter were cut from the plate. Each of the discs was then dimpled on one side and then ion-beam thinned on the same side. A Jeol-4000EX HRTEM was used to examine the specimens at 400 kV. Image simulation was performed using the *MUM* (*Melbourne University Multislice Algorithm Package*) image-simulation program.

3. Results and discussion

A through-focal series of experimental images of *o*-ZrO₂ is presented in Fig. 2. The imaging area is about 80 Å thick. Fig. 2(*a*), in which the black spots correspond to Zr-atom columns, closely resembles the structure image.

The Jeol-4000EX HRTEM has a spherical aberration (C_s) of 1 mm. At 400 kV, the Scherzer defocus is $\Delta f = -(C_s\lambda)^{1/2} =$

-404 Å (where λ is the electron wavelength) and the extended Scherzer (optimum) defocus is $\Delta f' \simeq -1.2\Delta f = -490$ Å. Calculations show that for ZrO₂, high black contrast at Zr-atom positions for a thin crystal occurs at the defocus around 400–450 Å. However, as crystal thicknesses increase, positions of the optimum defocus move from larger defocus values towards smaller defocus values as a result of dynamical phase changes in diffracted wave amplitudes (Lynch *et al.*, 1975). The specimen area for taking Fig. 2(*a*) is around 80 Å thick. Calculations show that the optimum defocus is about -260 Å for such a thickness.

Image simulations based on the three reported structures listed in Table 1 show that only the *Pbcm* structure perfectly matches the experimental images (inset of each micrograph, Fig. 2), and the orientation of the *o*-ZrO₂ shown in Fig. 2 was subsequently determined as [001].
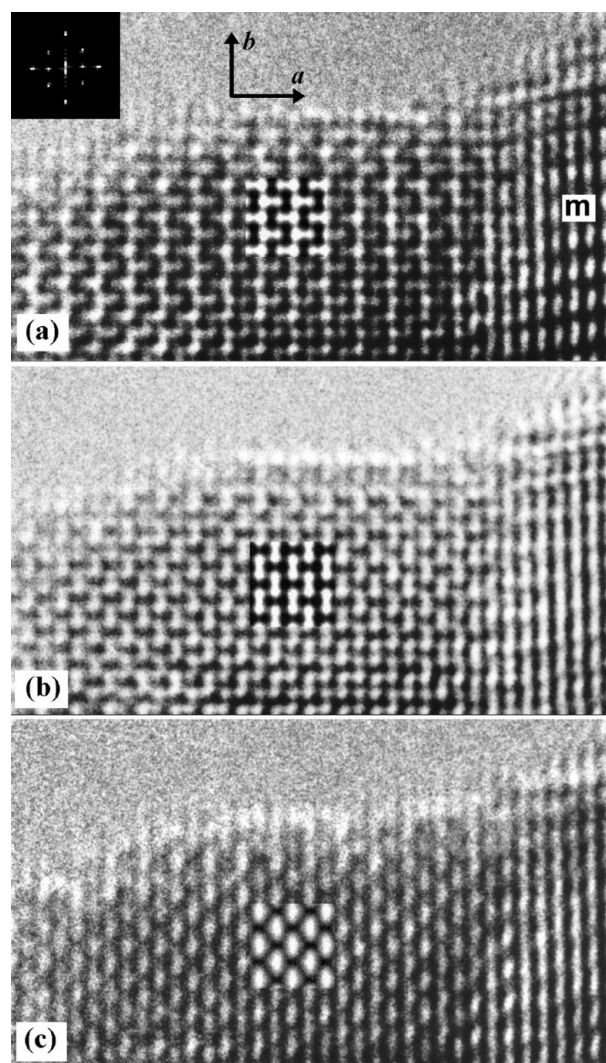

Figure 2
Through-focal series of images of *o*-ZrO₂ in [001] orientation. The right region of each micrograph shows the *m* phase already transformed from the *o* phase. The inset of each of the HRTEM images is a simulated image. (*a*) Image at optimum defocus around −260 Å. (*b*) Image at about −570 Å defocus. (*c*) Image at about −1200 Å defocus.
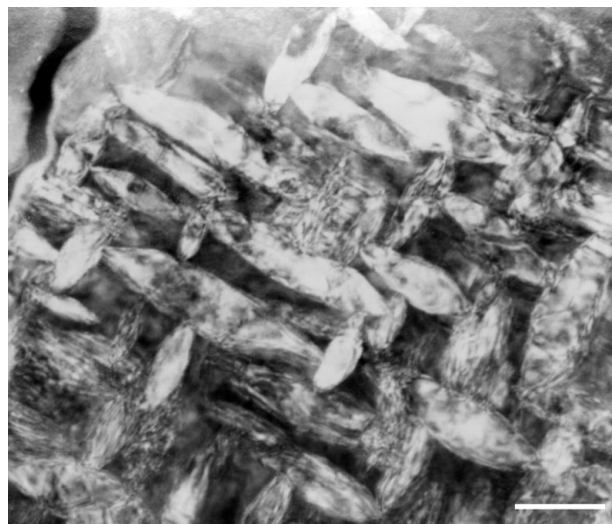

Figure 1
Dark-field image showing *o*-ZrO₂ particles in MgO-PSZ. The particles were initially *t*-ZrO₂ but were transformed to the *o* phase during specimen polishing and dimpling. Scale bar: 100 nm.

research papers

The unit cell of o-ZrO$_2$ with space group Pbcm, determined by Kudoh et al. (1987) (Table 1), contains four molecules of ZrO$_2$. Four Zr atoms occupy the 4d sites and four O atoms out of eight O atoms (denoted as O2) occupy 4c sites, while the remaining four O atoms (denoted as O1) occupy the 8e sites with equal probability. Fig. 3(a) schematically shows the positions of the Zr and O atoms in a unit cell projected on the ab plane. The four Zr atoms and two of the four O2 atoms are clearly shown in Fig. 3(a). Below each of the two O2 atoms there is one more O2 atom having the same x and y coordinates. Each of the O1 positions represents a pair of 8e sites with the same x and y coordinates. The lattice parameters are a = 0.5005 nm, b = 0.5235 nm and c = 0.5051 nm. A calculated image of the Pbcm structure is shown in Fig. 3(b). The four Zr atoms in a unit cell were marked and each of the dumbbell-like black sports corresponds to two Zr atom columns which have a spacing of 2.2 Å. As a comparison, the simulated structure images of o-ZrO$_2$ with space groups Pbc2$_1$ and Pbca are presented in Fig. 4.

The Pbcm structure contains a b-glide and therefore (0k0) reflections are kinematically forbidden for k odd (Fig. 3c and inset of Fig. 1a). These forbidden reflections remain forbidden dynamically under certain illumination conditions. One such illumination condition is when the incident-beam direction is aligned with the zone axis. Even for a small tilt away from the zone axis, these forbidden reflections can have significant intensities, and could result in misleading images in high-resolution imaging (Stone & Bursill, 1977; Smith et al., 1985). An experimental image showing the effect of crystal tilt is presented in Fig. 5. The specimen of the imaging area shown in Fig. 5 was bent. The central part of the imaging area is at zone axis [001], but both the left part and the right part of the central area are off this zone axis. The untilted area shows the real spacing of 2.5 Å, while at the tilted areas, the 3.6 Å periodicities dominate. The digital Fourier transform (inset) clearly shows the occurrence of the 010 and 0$\bar{1}$0 forbidden reflections.

4. Conclusions

By taking a through-focal series of HRTEM images, combined with image simulations, we have demonstrated that orthorhombic ZrO$_2$ formed in MgO-PSZ as a result of polishing and dimpling possesses the space group Pbcm. The Pbcm structure is one of the three possible space groups that orthorhombic can display. The structure image of orthorhombic ZrO$_2$ presented in this paper clearly shows the Zr atom positions of the Pbcm structure.
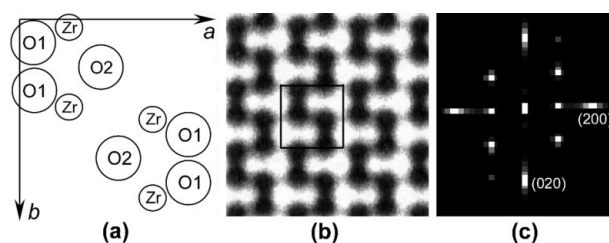
Figure 3
The Pbcm structure of o-ZrO$_2$. (a) Schematic representation of the positions of Zr and O atoms in a unit cell projected along the [001] orientation. (b) Calculated image at optimum defocus in the same orientation for a specimen thickness of 80 Å. The four Zr atoms in a unit cell are marked. (c) Fourier transform of the calculated image.
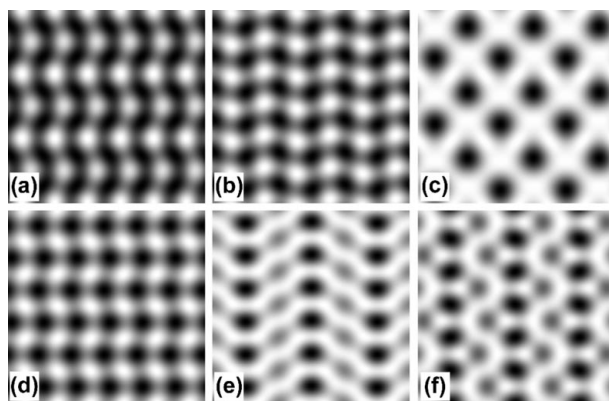

Figure 4
Simulated images of o-ZrO$_2$ with space group Pbc2$_1$ (a to c) and space group Pbca (d to f) for a specimen thickness of 80 Å at optimum defocus. All simulation conditions are the same as those used in calculating the image of the Pbcm structure, Fig. 3(b). In each of the images, areas with the darkest contrast correspond to the Zr-atom columns. (a) Pbc2$_1$ in [001], 3 × 3 unit cells. (b) Pbc2$_1$ in [100], 3 × 3 unit cells. (c) Pbc2$_1$ in [010], 3 × 3 unit cells. (d) Pbca in [100], 3 × 3 unit cells. (e) Pbca in [010], 1.5 × 3 unit cells. (f) Pbca in [001], 1.5 × 3 unit cells.
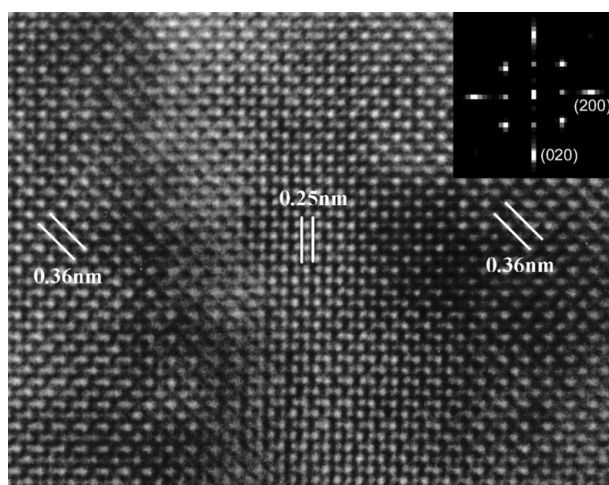

Figure 5
An experimental high-resolution image showing the effect of crystal tilt. The specimen of the imaging area was bent. The central area of the image is at zone axis [001], while the left side and right side regions were tilted with respective to this axis. The inset is the Fourier transform of the image, which shows the occurrence of the 010 and 0$\bar{1}$0 forbidden reflections due to crystal tilt.

References

Garvie, R. C., Hannink, R. H. J. & Mckinnon, N. A. (1981). US Patent No. 4 279 655.

Hannink, R. H. J. (1983). *J. Mater. Sci.* **18**, 457–70.

Hannink, R. H. J., Howard, C. J., Kisi, E. H. & Swain, M. V. (1994). *J. Am. Ceram. Soc.* **77**, 571–579.

Hill, R. J. & Reichert, B. E. (1990). *J. Am. Ceram. Soc.* **73**, 2822–2827.

Howard, C. J., Kisi, E. H. & Ohtaka, O. (1991). *J. Am. Ceram. Soc.* **74**, 2321–2323.

Kisi, E. H., Howard, C. J. & Hill, R. J. (1989). *J. Am. Ceram. Soc.* **72**, 1757–1760.

Kudoh, Y., Takeda, H. & Arashi, H. (1987). *Phys. Chem. Miner.* **13**, 233–237.

Liu, Z. & Spargo, A. E. C. (2001*a*). *Philos. Mag. A*, **81**, 625–636.

Liu, Z. & Spargo, A. E. C. (2001*b*). *J. Electron Microsc.* **50**, 443–446.

Liu, Z. (1999). PhD thesis, University of Melbourne.

Lynch, D. F., Moodie, A. F. & O'Keefe, M. A. (1975). *Acta Cryst.* A**31**, 300–307.

Marshall, D. B., James, M. R. & Porter, J. R. (1989). *J. Am. Ceram. Soc.* **72**, 218–227.

Ohtaka, O., Yamanoka, T., Kume, S., Hara, N., Asano, H. & Izumi, F. (1990). *Proc. Jpn Acad. Ser. B*, **66**, 193–196.

Smith, D. J., Bursill, L. A. & Wood, G. J. (1985). *Ultramicroscopy*, **16**, 19–31.

Stone, G. G. & Bursill, L. A. (1977). *Philos. Mag.* **35**, 1397–1412.

Suyama, R., Ashida, T. & Kume, S. (1985). *J. Am. Ceram. Soc.* **68**, C314–C315.